The Astrophysical Journal, 721:1383–1396, 2010 October 1 doi:10.1088/0004-637X/721/2/1383

FERMI GAMMA-RAY SPACE TELESCOPE OBSERVATIONS OF GAMMA-RAY OUTBURSTS FROM 3C 454.3 IN 2009 DECEMBER AND 2010 APRIL

M. Ackermann[1], M. Ajello[1], L. Baldini[2], J. Ballet[3], G. Barbiellini[4,5], D. Bastieri[6,7], K. Bechtol[1], R. Bellazzini[2], B. Berenji[1], R. D. Blandford[1], E. Bonamente[8,9], A. W. Borgland[1], J. Bregeon[2], M. Brigida[10,11], P. Bruel[12], R. Buehler[1], T. H. Burnett[13], S. Buson[6,7], G. A. Caliandro[14], R. A. Cameron[1], P. A. Caraveo[15], S. Carrigan[7], J. M. Casandjian[3], E. Cavazzuti[16], C. Cecchi[8,9], Ö. Çelik[17,18,19], A. Chekhtman[20,21], C. C. Cheung[20,22], J. Chiang[1], S. Ciprini[9], R. Claus[1], J. Cohen-Tanugi[23], S. Corbel[3,24], S. Cutini[16], F. D'Ammando[25,26], C. D. Dermer[20], A. de Angelis[27], F. de Palma[10,11], S. W. Digel[1], E. do Couto e Silva[1], P. S. Drell[1], R. Dubois[1], D. Dumora[28], L. Escande[28], C. Favuzzi[10,11], S. J. Fegan[12], E. C. Ferrara[17], L. Fuhrmann[29], Y. Fukazawa[30], P. Fusco[10,11], F. Gargano[11], D. Gasparrini[16], N. Gehrels[17], S. Germani[8,9], B. Giebels[12], N. Giglietto[10,11], P. Giommi[16], F. Giordano[10,11], M. Giroletti[31], T. Glanzman[1], G. Godfrey[1], I. A. Grenier[3], J. E. Grove[20], S. Guiriec[32], D. Hadasch[14], M. Hayashida[1], E. Hays[17], G. Jóhannesson[1], A. S. Johnson[1], W. N. Johnson[20], T. Kamae[1], H. Katagiri[30], J. Kataoka[33], J. Knödlseder[34], M. Kuss[2], J. Lande[1], S. Larsson[35,36,37], L. Latronico[2], S.-H. Lee[1], M. Llena Garde[35,36], F. Longo[4,5], F. Loparco[10,11], B. Lott[28], P. Lubrano[8,9], G. M. Madejski[1], A. Makeev[20,21], N. Marchili[29], M. N. Mazziotta[11], J. E. McEnery[17,38], J. Mehault[23], P. F. Michelson[1], T. Mizuno[30], C. Monte[10,11], M. E. Monzani[1], A. Morselli[39], I. V. Moskalenko[1], S. Murgia[1], T. Nakamori[33], K. Nalewajko[40], M. Naumann-Godo[3], P. L. Nolan[1], J. P. Norris[41], E. Nuss[23], T. Ohsugi[42], A. Okumura[43], N. Omodei[1], E. Orlando[44], J. F. Ormes[41], V. Pelassa[23], M. Pepe[8,9], M. Pesce-Rollins[2], F. Piron[23], T. A. Porter[1], S. Rainò[10,11], R. Rando[6,7], M. Razzano[2], A. Reimer[1,45], O. Reimer[1,45], L. C. Reyes[46], J. Ripken[35,36], S. Ritz[47], M. Roth[13], H. F.-W. Sadrozinski[47], D. Sanchez[12], A. Sander[48], J. D. Scargle[49], C. Sgrò[2], M. Sikora[40], E. J. Siskind[50], G. Spandre[2], P. Spinelli[10,11], M. S. Strickman[20], D. J. Suson[51], H. Takahashi[42], T. Takahashi[43], T. Tanaka[1], Y. Tanaka[43], J. B. Thayer[1], J. G. Thayer[1], D. J. Thompson[17], L. Tibaldo[3,6,7,59], D. F. Torres[14,52], G. Tosti[8,9], A. Tramacere[1,53,54], T. L. Usher[1], J. Vandenbroucke[1], N. Vilchez[34], V. Vitale[39,55], A. P. Waite[1], P. Wang[1], A. E. Wehrle[56], B. L. Winer[48], Z. Yang[35,36], T. Ylinen[36,57,58], and M. Ziegler[47]

[1] W. W. Hansen Experimental Physics Laboratory, Kavli Institute for Particle Astrophysics and Cosmology, Department of Physics and SLAC National Accelerator Laboratory, Stanford University, Stanford, CA 94305, USA
[2] Istituto Nazionale di Fisica Nucleare, Sezione di Pisa, I-56127 Pisa, Italy
[3] Laboratoire AIM, CEA-IRFU/CNRS/Université Paris Diderot, Service d'Astrophysique, CEA Saclay, 91191 Gif sur Yvette, France
[4] Istituto Nazionale di Fisica Nucleare, Sezione di Trieste, I-34127 Trieste, Italy
[5] Dipartimento di Fisica, Università di Trieste, I-34127 Trieste, Italy
[6] Istituto Nazionale di Fisica Nucleare, Sezione di Padova, I-35131 Padova, Italy
[7] Dipartimento di Fisica "G. Galilei," Università di Padova, I-35131 Padova, Italy
[8] Istituto Nazionale di Fisica Nucleare, Sezione di Perugia, I-06123 Perugia, Italy
[9] Dipartimento di Fisica, Università degli Studi di Perugia, I-06123 Perugia, Italy
[10] Dipartimento di Fisica "M. Merlin" dell'Università e del Politecnico di Bari, I-70126 Bari, Italy
[11] Istituto Nazionale di Fisica Nucleare, Sezione di Bari, 70126 Bari, Italy
[12] Laboratoire Leprince-Ringuet, École polytechnique, CNRS/IN2P3, Palaiseau, France
[13] Department of Physics, University of Washington, Seattle, WA 98195-1560, USA
[14] Institut de Ciencies de l'Espai (IEEC-CSIC), Campus UAB, 08193 Barcelona, Spain
[15] INAF-Istituto di Astrofisica Spaziale e Fisica Cosmica, I-20133 Milano, Italy
[16] Agenzia Spaziale Italiana (ASI) Science Data Center, I-00044 Frascati (Roma), Italy
[17] NASA Goddard Space Flight Center, Greenbelt, MD 20771, USA
[18] Center for Research and Exploration in Space Science and Technology (CRESST) and NASA Goddard Space Flight Center, Greenbelt, MD 20771, USA
[19] Department of Physics and Center for Space Sciences and Technology, University of Maryland Baltimore County, Baltimore, MD 21250, USA
[20] Space Science Division, Naval Research Laboratory, Washington, DC 20375, USA; charles.dermer@nrl.navy.mil
[21] George Mason University, Fairfax, VA 22030, USA
[22] National Research Council Research Associate, National Academy of Sciences, Washington, DC 20001, USA
[23] Laboratoire de Physique Théorique et Astroparticules, Université Montpellier 2, CNRS/IN2P3, Montpellier, France
[24] Institut universitaire de France, 75005 Paris, France
[25] IASF Palermo, 90146 Palermo, Italy
[26] INAF-Istituto di Astrofisica Spaziale e Fisica Cosmica, I-00133 Roma, Italy
[27] Dipartimento di Fisica, Università di Udine and Istituto Nazionale di Fisica Nucleare, Sezione di Trieste, Gruppo Collegato di Udine, I-33100 Udine, Italy
[28] Centre d'Études Nucléaires de Bordeaux Gradignan, Université Bordeaux 1, CNRS/IN2P3, 33175 Gradignan, France; escande@cenbg.in2p3.fr, lott@cenbg.in2p3.fr
[29] Max-Planck-Institut für Radioastronomie, Auf dem Hügel 69, 53121 Bonn, Germany
[30] Department of Physical Sciences, Hiroshima University, Higashi-Hiroshima, Hiroshima 739-8526, Japan
[31] INAF Istituto di Radioastronomia, 40129 Bologna, Italy
[32] Center for Space Plasma and Aeronomic Research (CSPAR), University of Alabama in Huntsville, Huntsville, AL 35899, USA
[33] Research Institute for Science and Engineering, Waseda University, 3-4-1, Okubo, Shinjuku, Tokyo 169-8555, Japan
[34] Centre d'Étude Spatiale des Rayonnements, CNRS/UPS, BP 44346, F-30128 Toulouse Cedex 4, France
[35] Department of Physics, Stockholm University, AlbaNova, SE-106 91 Stockholm, Sweden
[36] The Oskar Klein Centre for Cosmoparticle Physics, AlbaNova, SE-106 91 Stockholm, Sweden
[37] Department of Astronomy, Stockholm University, SE-106 91 Stockholm, Sweden
[38] Department of Physics and Department of Astronomy, University of Maryland, College Park, MD 20742, USA
[39] Istituto Nazionale di Fisica Nucleare, Sezione di Roma "Tor Vergata," I-00133 Roma, Italy
[40] Nicolaus Copernicus Astronomical Center, 00-716 Warsaw, Poland
[41] Department of Physics and Astronomy, University of Denver, Denver, CO 80208, USA

[42] Hiroshima Astrophysical Science Center, Hiroshima University, Higashi-Hiroshima, Hiroshima 739-8526, Japan
[43] Institute of Space and Astronautical Science, JAXA, 3-1-1 Yoshinodai, Sagamihara, Kanagawa 229-8510, Japan; tanaka@astro.isas.jaxa.jp
[44] Max-Planck Institut für extraterrestrische Physik, 85748 Garching, Germany
[45] Institut für Astro- und Teilchenphysik and Institut für Theoretische Physik, Leopold-Franzens-Universität Innsbruck, A-6020 Innsbruck, Austria
[46] Kavli Institute for Cosmological Physics, University of Chicago, Chicago, IL 60637, USA
[47] Santa Cruz Institute for Particle Physics, Department of Physics and Department of Astronomy and Astrophysics, University of California, Santa Cruz, CA 95064, USA
[48] Department of Physics, Center for Cosmology and Astro-Particle Physics, The Ohio State University, Columbus, OH 43210, USA
[49] Space Sciences Division, NASA Ames Research Center, Moffett Field, CA 94035-1000, USA
[50] NYCB Real-Time Computing Inc., Lattingtown, NY 11560-1025, USA
[51] Department of Chemistry and Physics, Purdue University Calumet, Hammond, IN 46323-2094, USA
[52] Institució Catalana de Recerca i Estudis Avançats (ICREA), Barcelona, Spain
[53] Consorzio Interuniversitario per la Fisica Spaziale (CIFS), I-10133 Torino, Italy
[54] INTEGRAL Science Data Centre, CH-1290 Versoix, Switzerland
[55] Dipartimento di Fisica, Università di Roma "Tor Vergata," I-00133 Roma, Italy
[56] Space Science Institute, Boulder, CO 80301, USA
[57] Department of Physics, Royal Institute of Technology (KTH), AlbaNova, SE-106 91 Stockholm, Sweden
[58] School of Pure and Applied Natural Sciences, University of Kalmar, SE-391 82 Kalmar, Sweden
Received 2010 July 2; accepted 2010 August 3; published 2010 September 9

ABSTRACT

The flat spectrum radio quasar 3C 454.3 underwent an extraordinary outburst in 2009 December when it became the brightest γ-ray source in the sky for over 1 week. Its daily flux measured with the *Fermi*-Large Area Telescope at photon energies $E > 100$ MeV reached $F_{100} = 22 \pm 1 \times 10^{-6}$ photon cm^{-2} s^{-1}, representing the highest daily flux of any blazar ever recorded in high-energy γ-rays. It again became the brightest source in the sky in 2010 April, triggering a pointed-mode observation by *Fermi*. The correlated γ-ray temporal and spectral properties during these exceptional events are presented and discussed. The main results show flux variability over time scales less than 3 hr and very mild spectral variability with an indication of gradual hardening preceding major flares. The light curves during periods of enhanced activity in 2008 July–August and 2010 December show strong resemblance, with a flux plateau of a few days preceding the major flare. No consistent loop pattern emerged in the γ-ray spectral index versus the flux plane as would be expected in acceleration and cooling scenarios. The maximum energy of a photon from 3C 454.3 is $\approx$20 GeV and a minimum Doppler factor of $\approx$13 is derived. The γ-ray spectrum of 3C 454.3 shows a significant spectral break between $\approx$2 and 3 GeV that is very weakly dependent on the flux state, even when the flux changes by an order of magnitude.

Key words: galaxies: active – gamma rays: galaxies – quasars: individual (3C 454.3)

Online-only material: color figures

1. INTRODUCTION

The radio source 3C 454.3 is a well-known flat spectrum radio quasar (FSRQ) at redshift $z = 0.859$. It entered a bright phase starting in 2000 and has shown remarkable activity in the past decade. It underwent major outbursts in 2005, reaching an *R*-band magnitude of 12.0 and the largest apparent optical luminosity ever recorded from a blazar (Fuhrmann et al. 2006; Villata et al. 2006; Giommi et al. 2006). It also underwent major outbursts in 2007 (Ghisellini et al. 2007; Vercellone et al. 2009a) and 2008 (Vercellone et al. 2010; Jorstad et al. 2010).

First observations of 3C 454.3 with the *Fermi*-Large Area Telescope (LAT) began in 2008 July during *Fermi*'s commissioning period, when the source was found at a high flux state with $F_{E>100\,\mathrm{MeV}} \cong 10 \times 10^{-6}$ photon cm^{-2} s^{-1} (Abdo et al. 2009). During this time, most observations were carried out in a pointed mode with 3C 454.3 being close to the edge of the field of view ($\simeq$55° off-axis), which did not allow for detailed spectral analysis during the brightest stage of the outburst. Observations in the decay stage, performed in the survey mode, revealed a timescale less than 2 d for the flux to decline by a factor of 2. The spectrum showed a spectral break around 2 GeV with a spectral steepening from $\Gamma_1 = 2.3$ to $\Gamma_2 = 3.5$. Such a break has now been found to be a common feature in bright FSRQs and in some low-synchrotron peaked BL Lacertae objects as well (Abdo et al. 2010d). Based on weekly light curves, a very moderate "harder when brighter" effect has also been observed, with the photon spectral index obtained with a single power-law (PL) fit varying by less than 0.3 for flux ratios varying by >7 (Abdo et al. 2010d). The source is listed as 1FGL J2253.9+1608 in the First-LAT active galactic nucleus (AGN) catalog (Abdo et al. 2010b).

Because of its brightness, 3C 454.3 is the first source for which daily resolved broadband spectral energy distributions (SEDs) with GeV data have been obtained (e.g., Abdo et al. 2009; Bonnoli et al. 2010). This offers a wealth of information on the source's spectral states. For example, the γ-ray emission has been observed to correlate with the optical and X-ray bands, pointing to the presence of a single emission zone (Bonning et al. 2009b; Bonnoli et al. 2010), with no significant lag between optical and γ-rays. Strong Lyα radiation has been observed from 3C 454.3 (Bonnoli et al. 2010), providing an external photon source for Compton scattering along with torus emission (Sikora et al. 2009). Modeling of such SEDs with single-zone models has been performed to derive jet powers, with Compton-scattered components from the accretion disk and the broad-line region (BLR; Finke & Dermer 2010). Bonnoli et al. (2010) studied the single-day broadband SEDs in the bright flare discussed here and in a lower state and found that a single-zone

[59] Partially supported by the International Doctorate on Astroparticle Physics (IDAPP) program.

external Compton (EC) from the disk, X-ray corona, and torus plus synchrotron self-Compton (SSC) model adequately fitted the data. However, with a similar analysis using AGILE data, Pacciani et al. (2010) came to the conclusion that an additional component was required to fit the data.

The differential distribution of the fluxes of the daily light curves, measured over 18 months, increases as $F^{1.5}$ for low fluxes and peaks around $F[E>100\ \mathrm{MeV}] \simeq 3\times10^{-6}$ photon cm^{-2} s^{-1} and the fraction of the time where the source reaches a flux greater than 10 times the average flux is only 1% (Tavecchio et al. 2010). Foschini et al. (2010) claim γ-ray variability from 3C 454.3 on timescales as short as a few hours from the LAT data and implications on the size and distance to the black hole of the emitting region were discussed by Tavecchio et al. (2010). The results from the flaring state discussed above (as well as those presented in this paper) cannot be seen as typical for this source, as 3C 454.3's level of activity was much lower during the EGRET era, when its mean flux was $F[E>100\ \mathrm{MeV}] \simeq 5.4\times10^{-7}$ photon cm^{-2} s^{-1} (Hartman et al. 1999).

The continuous monitoring by the *Fermi*-LAT showed that the source activity faded continuously in early 2009 and then rose back up from June onward. It underwent an exceptional outburst in 2009 November–2010 January when it became the brightest γ-ray source in the sky for over a week, reaching a record daily flux level in the GeV band as seen by the LAT and AGILE (Striani et al. 2009a, 2009b; Escande & Tanaka 2009; Striani et al. 2010). At the same time, it also showed strong activity at optical frequencies (Villata et al. 2009; Bonning et al. 2009a; Sasada et al. 2009), in the *Swift*/XRT and *Swift*/BAT bands (Sakamoto et al. 2009; Krimm et al. 2009), and in the *INTEGRAL*/IBIS band (Vercellone et al. 2009b). Although its γ-ray flux reached record levels, the γ-ray luminosity did not, as larger luminosities have been observed for blazars located at larger distances such as PKS 1622-297 (Mattox et al. 1997). During the brightest flares, the power corresponding to the γ-ray luminosity was found to be similar to or greater than the accretion power of the disk (Bonnoli et al. 2010).

The source remained active afterward with a slowly decaying flux around 2×10^{-6} photon cm^{-2} s^{-1} until early 2010 April, when it brightened up again to a flux level of $\approx16\times10^{-6}$ photon cm^{-2} s^{-1}, prompting the first *Fermi*-LAT target-of-opportunity (ToO) pointed observation beginning on MJD 55,291 (2010 April 5) lasting for 200 ks.

These two major events offer a unique opportunity to probe intra-day variability and the associated spectral changes in the γ-ray band, which is the focus of this paper. Particular attention is paid to the correlated spectral/flux variations on different time scales, both in terms of spectral hardness and position of the spectral break, which have not been investigated in detail before. In Section 2, observations and analysis of data from 3C 454.3 from 2009 August through 2010 April are presented. Section 3 gives results of the analysis and Section 4 provides interpretation. We summarize in Section 5. A flat ΛCDM cosmology with $H_0 = 71$ km s^{-1} Mpc^{-1}, $\Omega_m = 0.27$, $\Omega_\Lambda = 0.73$ is used in this paper, implying a luminosity distance $d_L = 1.69\times10^{28}$ cm to 3C 454.3.

2. OBSERVATIONS AND ANALYSIS

The *Fermi*-LAT is a pair-conversion γ-ray telescope sensitive to photon energies greater than 20 MeV. In its nominal scanning mode, it surveys the whole sky every 3 hr with a field of view of about 2.4 sr (Atwood et al. 2009). The data presented in this paper (restricted to the 100 MeV–200 GeV range) were collected from MJD 55,070 (2009 August 27) to MJD 55,307 (2010 April 21) in the survey mode, except for a 200 ks period starting at MJD 55,291.82 (2010 April 5 19:38 UT) when the pointed mode was used, resulting in a gain of rate of accumulation of exposure by about a factor of 3.5 over the survey mode. During the pointed mode, the source direction was offset by 10° with respect to the LAT axis in order to limit adverse effects related to gaps in the detector that can affect on-axis photons. Over 3000 photons with $E > 100$ MeV were collected in the pointed mode. To minimize systematics, only photons with energies greater than 100 MeV were considered in this analysis. In order to avoid contamination from Earth limb gamma-rays, a selection of events with zenith angle <105° was applied. This analysis was performed with the standard analysis tool *gtlike*, part of the *Fermi*-LAT ScienceTools software package (ver. v9r15p5). The P6_V3_DIFFUSE set of instrument response functions was used. This set includes a correction for the average reduction of the effective area due to pile-up effects as fewer photon events pass the rejection cuts. This correction is sufficient for integration times longer than a day. The residual energy and trigger-rate-dependent acceptance variations present for shorter times as established with Vela and Galactic diffuse emission data (typically amounting to less than 10% in the considered periods), have not been corrected for in this analysis.

Photons were selected in a circular region of interest (ROI) 10° in radius, centered at the position of 3C 454.3. The isotropic background, including the sum of residual instrumental background and extragalactic diffuse γ-ray background, was modeled by fitting this component at high galactic latitude (file provided with ScienceTools). The Galactic diffuse emission model version "gll_iem_v02.fit," was used, with both flux and photon spectral index left free in the fit (the Galactic longitude and latitude of 3C 454.3 are 86.°1 and −38.°2, respectively). All point sources lying within the ROI and a surrounding 5° wide annulus with a flux greater than about 1% of the quiescent level of 3C 454.3 were modeled in the fit with single PL distributions.

Although the actual spectral shape is better reproduced by a broken power law (BPL), the spectral variations were investigated using the photon indices resulting from single PL fits, as these indices are determined with a lower statistical uncertainty than those obtained from BPL fits. All light curves were produced using fluxes derived with PL fits.

Different analyses were performed by fitting the spectra with various models over the whole energy range covered by the LAT at $E > 100$ MeV: a BPL $N(E) = N_0(E/E_{\mathrm{break}})^{-\Gamma_i}$, with $i = 1$ if $E < E_{\mathrm{break}}$ and $i = 2$ if $E > E_{\mathrm{break}}$, a log parabola function ($N(E) = N_0(E/E_p)^{-\alpha-\beta\log(E/E_p)}$ where E_p is fixed at 1 GeV) and a PL with exponential cutoff function ($N(E) = N_0(E/E_0)^{-\Gamma}\exp(-E/E_{\mathrm{cutoff}})$), and with a PL model over equally spaced logarithmic energy bins with the spectral index kept constant and equal to the value fitted over the whole range.

In case of fits with BPL models, the break energy (E_{break}), which separates the photon energy ranges where different photon indices Γ_1 (for $E < E_{\mathrm{break}}$) and Γ_2 (for $E > E_{\mathrm{break}}$) apply, could not be obtained directly from the fit because of convergence problems due to the non-smooth character of the BPL function at the break energy. It was instead computed from a log-likelihood profile fitting procedure, with a statistical uncertainty corresponding to a difference of $-2\Delta L = 1$ in the log-likelihood function L with respect to its minimum.

In order to minimize spurious correlations between flux and spectral index, the fluxes $F_{E>E_1}$ were also computed above

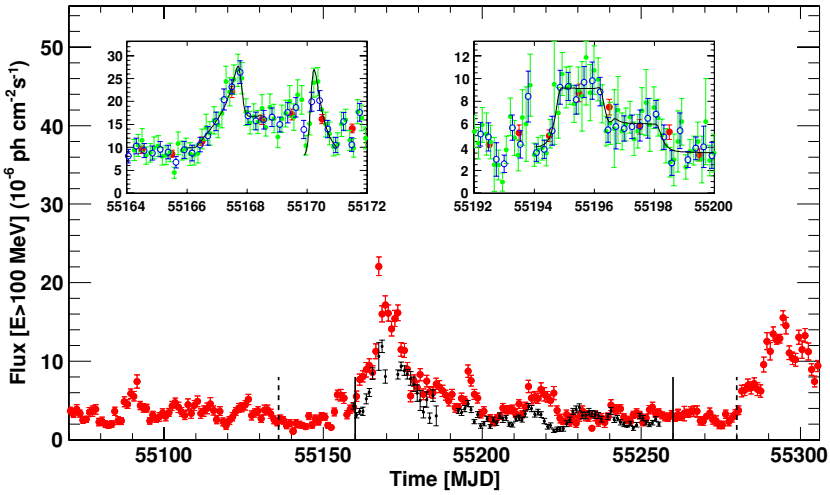

Figure 1. Light curve of the flux of 3C 454.3 in the 100 MeV–200 GeV band (red) between MJD 55,070–55,307 (2009 August 27–2010 April 21). The solid (dashed) lines mark the period over which the PSD (CWT) analysis has been conducted. The light curve of the 2008 July–August flare, shifted by 511 d, is shown for comparison (black). The insets show blow-ups of the two periods when the largest relative flux increases took place. The red, blue, and green data points in the insets correspond to daily, 6 hr, and 3 hr averaged fluxes, respectively. The fit results discussed in the text are displayed as solid curves.

(A color version of this figure is available in the online journal.)

the photon energy E_1 where the correlation between integrated flux and index is minimal. This energy was derived from a PL fit of the form $N(E) = F_{E>E_0}(\Gamma - 1)\, E^{-\Gamma}/E_0^{-\Gamma+1}$ (with E_0=100 MeV). Since $F_{E>E_1} = F_{E>E_0}(E_1/E_0)^{-\Gamma+1}$, minimizing $\Delta F_{E>E_1}/F_{E>E_1}$ with respect to E_1 yields $\ln(E_1/E_0) = C_{F\Gamma}/(F_{E>E_0}\, C_{\Gamma\Gamma})$, where $C_{F\Gamma}$ and $C_{\Gamma\Gamma}$ are terms of the covariance matrix returned by the fit. In the 3C 454.3 case, E_1 has been found to be 163 MeV over the ToO time range. The same value has been used for the other time periods as well.

The estimated systematic uncertainty on the flux is 10% at 100 MeV, 5% at 500 MeV, and 20% at 10 GeV. The energy resolution is better than 10% over the range of measured $E_{\rm break}$.

3. RESULTS

Figure 1 displays the daily light curves (red points) from MJD 55,070 to 55,307 (2009 August 27–2010 April 21) for fluxes above 100 MeV. The periods showing the fastest flux variations during the December flare, with fluxes changing by more than a factor of 2 in amplitude, are enlarged in the insets, with the $E > 100$ MeV fluxes averaged over a daily, 6 hr, and 3 hr binning shown by the red, open blue, and green data points, respectively. The error bars are statistical only. Three flares displaying a flux variation greater than a factor of 2 over less than a day (MJD 55,167, 55,170, and 55,195) have been studied extensively during this period. These flares exhibit very different profiles and degrees of symmetry. The first two flares were fitted with the function (Abdo et al. 2010a)

$$F = 2F_0(e^{(t_0-t)/T_r} + e^{(t-t_0)/T_f})^{-1} + F_{\rm bgd}(t), \qquad (1)$$

where T_r and T_f are the rising and falling times, F_0 is the flare flux amplitude, and $F_{\rm bgd}(t)$ is a (slowly varying) background flux, while for the third one a constant plateau flux was allowed between the rising and falling phases. The characteristic flare duration can be estimated as T_r+T_f. We obtained $T_r = 0.37$ d and $T_f = 0.06$ d for the MJD 55,167 (December 2) flare, and $T_r = 0.07$ d and $T_f = 0.26$ d for the MJD 55,170 (December 5) flare. The MJD 55,195 flare, which is less prominent, shows a rise time of $\simeq$0.16 d. In the two early flares, the flux variation F_0 was greater than 10^{-5} photon (>100 MeV) cm^{-2} s^{-1}, and statistically significant factor of 2 variations take place on timescales as short as 3 hr.

In Figure 1, the light curve of the 2008 July–August outburst (shifted by 511 d; see Abdo et al. 2009) is shown for comparison. The resemblance of the two light curves is notable, although the estimated fluences are different by 40%. The brightest periods of the outbursts last for about 10 d and are then followed by a long tail of fairly high activity upon which are superimposed minor flares lasting for a few days. Although the outburst in 2010 April is longer, lasting for > 30 d, it exhibits similar patterns as the 2009 December outburst, where its maximum level is preceded by an intermediate elevated flux lasting for about 5 d. This feature could serve as an alert for an imminent surge in flux.

The power density spectrum (PDS) of the MJD 55,140–552, 603 hr light curve has been calculated in a similar way as that reported in Abdo et al. (2010a) for the 11 month light curve (3 d bin), normalized to fractional variance per frequency unit (f) and white-noise subtracted. The time period is marked by lines in Figure 1. This PDS indicates a PL power density, $1/f^a$ with index $a = 1.50 \pm 0.06$, i.e., intermediate between flickering (red noise) and shot noise (driven by Brownian processes). Such a result confirms over a wider frequency range the value found with the first 11 months of data. In Figure 2, the first-order structure function (SF), the PDS, and the Morlet continuous wavelet transform (CWT) of the continuous, unprecedented-resolution, γ-ray light curve of MJD 55,140–55,260 are reported. A break around 6.5 d is suggested by the SF analysis, the power-index slopes being $a = 1.29 \pm 0.10$ between 3 hr and 6.5 d, and $a = 1.64 \pm 0.10$ between 6.5 and about 26 d, while at longer lags spurious drops due to the finite range become apparent. The PDS analysis confirms these values ($a = 1.40 \pm 0.19$ at high frequency and $a = 1.56 \pm 0.18$ at low frequency). The temporal behavior of 3C 454.3 is therefore showing $1/f^{1.5}$ universality from 3 hr to 11 month timescales. The 6.5 d break, consistently confirmed by the PSD and more clearly depicted by the SF, represents a steepening toward longer lags (flattening toward higher frequencies) and does not necessarily imply a local characteristic time scale, as it could simply be the point where two PDS components with different slopes are equally strong. Gamma-ray variability in

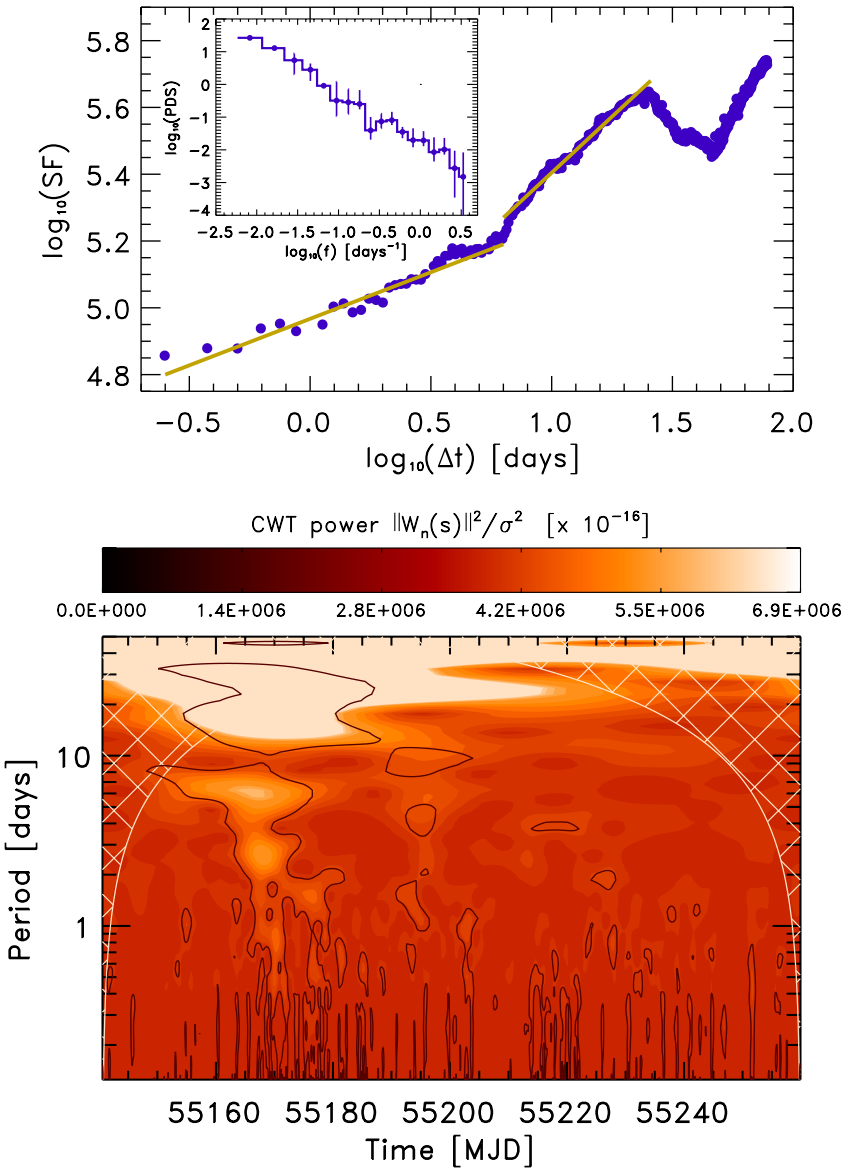

Figure 2. Top panel: SF of the 3 hr bin flux light curve for the period MJD 55,140–55,260 and corresponding PDS (inset). Bottom panel: plane contour plot of the continuous Morlet wavelet transform power density for the same light curve. Thick black contours are the 90% confidence levels of true signal features against white/red noise background, and cross-hatched regions represent the "cone of influence," where spurious edge effects become important.

(A color version of this figure is available in the online journal.)

3C 454.3 can be seen as a short-term realization of a stochastic mechanism, where structures that are resolved in shorter observations are simply averaged out in long observations, and where big outbursts correspond to statistical tails of the same process.

The CWT in Figure 2 provides a local and detailed time series analysis, through the two-dimensional energy density function (modulus of the transform, filled color contour) computed using a Morlet waveform, providing the best tradeoff between localization and period/frequency resolution. For timescales below 1 d no local peaks are found, although some marginal features in this time range are found during the outburst state. The big outburst of 2009 December is, in fact, localized and decomposed in a chain of well-defined power CWT peaks. The 6.5 d timescale is confirmed by the major peak out of the cone of influence (localized at about MJD 55,166, i.e., the onset of the outburst, MJD $\sim$ 55,166.2–55,172). A second energetic peak in this period is found at about 2.5 d manifesting another dominating timescale during the outburst, while in the second period of the outburst two minor power peaks at about 19 hr and 1.3 d are also visible. Based on this CWT local analysis, there is no evidence for structure on timescales shorter than about 12 hr but shorter timescales close to the sampling scale cannot be ruled out.

The 1 GeV daily light curve, shown in Figure 3 (top), closely resembles the 100 MeV light curve, hinting at little spectral variability. This behavior is confirmed by the very limited variation of the photon spectral index measured at $E > E_1 = 163$ MeV, displayed in Figure 3 (bottom) by the daily average photon index (open blue symbols) as well as the weekly averaged ones (solid black points). The near constancy of the spectrum is in accord with the results found from the 2008 July flare and the first 6 months of LAT data (Abdo et al. 2009, 2010d).

The variation of the amplitude of the weekly photon indices is only $\Delta\Gamma = 0.35$ (varying between 2.35 and 2.7) during the period under consideration, but the variation is statistically significant.

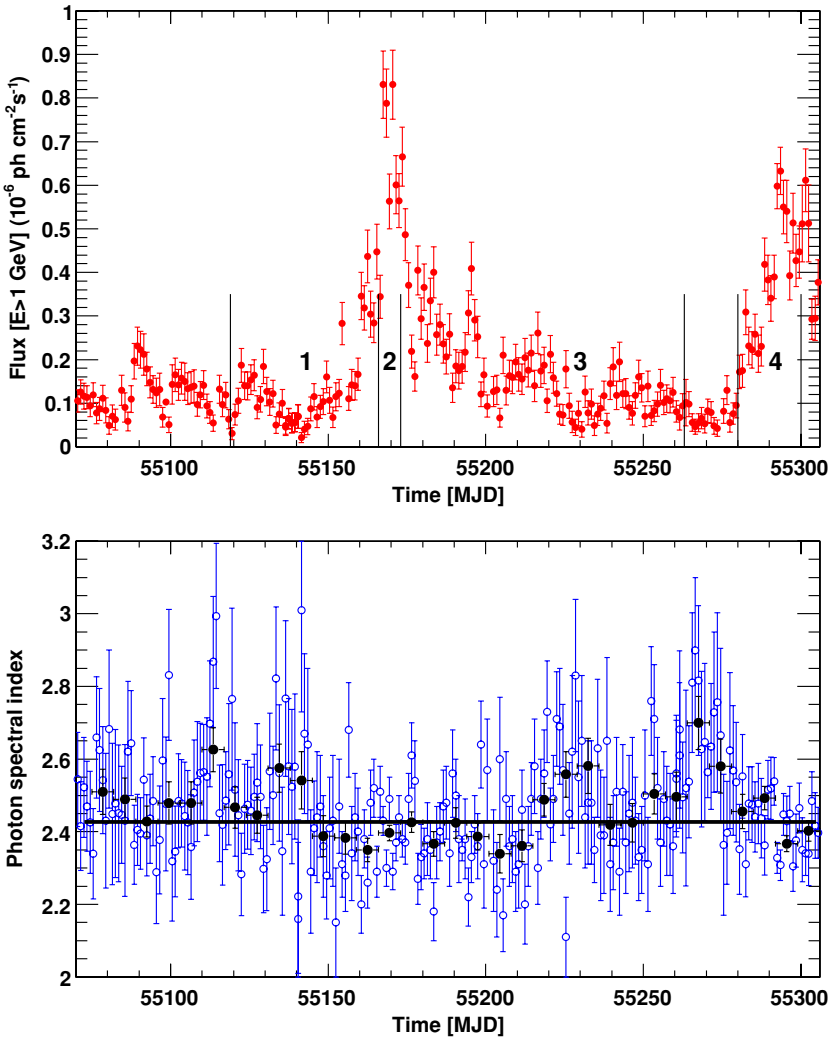

Figure 3. Top: light curve of the flux in the 1 –200 GeV band. Bottom: variation of the daily (blue points) and weekly (black points) photon spectral index derived from a PL fit. The black line depicts the mean weekly spectral index.
(A color version of this figure is available in the online journal.)

Comparing the weekly photon indices to their weighted average returns a reduced $\chi^2 = 86.4/32$, corresponding to a 10^{-7} probability for a nonvariable signal. Particularly notable is a slight softening of the spectrum during the periods of lowest fluxes, particularly during the periods of MJD 55,221–55,235 and 55,264–55,278. There is also a suggestion that a progressive hardening over several weeks precedes a major outburst, but more such events will be needed to establish whether this behavior is typical.

The correlation between photon index and flux was further investigated by computing a discrete cross-correlation function (DCCF) following Edelson & Krolik (1988). Error estimates were obtained by a Monte Carlo method (Peterson et al. 1998). The DCCF for the time of the December outburst and its decay (MJD 55,136–55,280) show evidence for a time lag such that index variations lead the flux by about 7 d. The photon flux above 163 MeV was used for this analysis. As stated above the light curve and photon index plots indicate a spectral softening at low flux levels. We therefore calculated a DCCF also using the logarithm of the flux, which is less dominated by the high flux values. The DCCF for this case (see Figure 4) gives a somewhat stronger correlation than for linear flux, supporting the impression that spectral softening at low flux levels has a clear contribution to the correlation. The time lag of the correlation peak, estimated by fitting a Gaussian function, was -6.8 ± 2.8 d when log(flux) was used and -7.9 ± 3.7 d for linear flux. As error values we used the standard deviation of Gaussian fits to the DCCF of Monte Carlo simulations, again along the lines of Peterson et al. (1998). As an additional test of the significance we divided the flare light curve into three segments (MJD 55,136–55,190, 55,190–55,240, and 55,240–55,280), each of which showed a time lag similar to that of the overall data. In contrast, the correlation during the 2010 April flare is weak and if anything shows a lag in the opposite sense. On the other hand, the data from the 2008 flare of this source do exhibit a time lag (-5.6 ± 3.4 d) similar to that of the 2009 December flare. The main uncertainty in the DCCF analysis is the possibility of spurious correlations. The fact that a similar time lag is seen in a number of independent data sets gives support for the, still tentative, detection of a lag between the flux and photon-index variations.

Figure 5, top left (right) presents the weekly (daily) averaged PL photon spectral index versus flux above E_1 (the photon energy where the correlation between integrated flux and index is minimal). A weak "harder when brighter" effect shows up for weekly bins, but is almost washed out when considering

daily bins. To make the trend clearer, photons were sorted in three daily-flux bins (F_{E_1} <2.5, 2.5 < F_{E_1} < 5, and 5 < F_{E_1} < 10, where F_{E_1} is the photon flux above E_1 in units of 10^{-6} photon cm^{-2} s^{-1}) and the analysis was repeated with the resulting photon files. The result, displayed as red points in the top right panel of Figure 5, still exhibits a slight harder when brighter effect. The data point at $F_{E_1} \cong 11$ corresponds to the MJD 55,167 flare and is consistent with the trend observed at lower flux. The three other panels in Figure 5 show the photon spectral index versus flux patterns for the three rapid flares, obtained either with a 6 hr binning (middle left and bottom left) or a 3 hr binning (middle right). The light curves at $E > E_1$ (not above 100 MeV, as in Figure 1) calculated at the time of the main flaring episodes are displayed in the insets of Figure 1. Despite the flux reaching the highest values for a non-gamma-ray burst (GRB) cosmic source, the statistical significance of these patterns is marginal, except for the MJD 55,167 flare. Instead of a well-defined, universal pattern, a variety of patterns is found. The MJD 55,167 flare is associated with a clockwise pattern, with a flux-doubling accompanied by an essentially constant (or weakly harder) photon spectral index. The reduced χ^2 for a constant fit of the photon spectral index is 28.6/9. The pattern is somewhat indicative of a "hard-lag" effect possibly reflecting particle acceleration (Kirk & Mastichiadis 1999). The short MJD 55,170 flare shows an indication for a counterclockwise loop ($\chi^2_r = 6.0/7$). The loop diagram for this flare on 3 hr timescales reveals the simplest ordered pattern, in this case a softening followed by a flux increase which then decays in flux and hardness. This could reflect the underlying timescale on which coherent variability takes place in 3C 454.3. Because this pattern does not recur in other flaring episodes, no strong conclusions can be made, however. The MJD 55,195 flare shows some softening during the plateau (points 3–6) following the flux rise as expected from a cooling behavior, but the significance is low ($\chi^2_r = 8.6/9$). While it is difficult to draw any firm conclusion on acceleration and cooling from these patterns, the lack of strong spectral variability still provides clues to the underlying physical processes.

Figure 6 shows the flux and photon spectral index as a function of time in the period around (blue symbols) and during (red symbols) the time of the ToO when the *Fermi*-LAT was in the pointed mode (MJD 55,291.82–55,294.13). The binning is 6 hr and 3 hr for the survey and pointed modes, respectively. As expected by the 3.5-fold increase in exposure per unit time during the ToO, the statistical accuracy in the measurement of both parameters improves significantly. Although in a high state, the source was unfortunately fairly steady during this period. No indication for variability more rapid than that observed during the giant outburst is found during the ToO period, as already noted by Foschini et al. (2010). The photon spectral index versus flux above E_1 measured in 3 hr time bins is plotted in Figure 7. The time sequence is indicated by labels, the first and last points of the sequence being labeled as well in the light curve of Figure 6. The reduced χ^2 for a constant fit of the photon spectral index is 18.52/16, indicating that the data are consistent with a constant value. The correlation coefficient is 0.26.

Figure 8 shows the integrated spectrum from Period 1, MJD 55,121–55,165; Period 2, MJD 55,166–55,173 (week of the giant outburst); Period 3, MJD 55,174–55,262; Period 4, MJD 55,280–55,300. The distributions have been fitted with a BPL, a log parabola function, and a PL with exponential cutoff function. The log parabola gives a worse fit than the BPL and the PL with exponential cutoff functions, which are difficult to discriminate

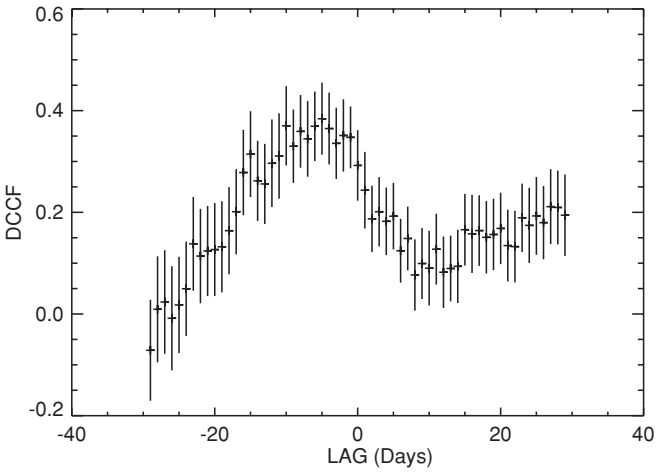

Figure 4. DCCF between photon index and log(flux) for the time of the 2009 December flare and its decay. The peak at −7 d suggests that index variations may lead the flux by about 1 week.

for these periods. The fitted parameters are given in Tables 1–3 for the four periods.

The variation of break energy (cutoff energy) with flux is displayed in the left (right) panel in Figure 9 at different observing periods. No strong evolution of either the break energy or the cutoff energy is found, but there is some indication of a slight hardening with flux. For a given flux, the position of the break energy is slightly different from that observed during the bright outburst in 2008, but all $E_{\rm break}$ (and $E_{\rm cutoff}$) are constant within a factor of ≈2. For the same periods, Striani et al. (2010) found fairly large spectral variability with the AGILE data, with a photon spectral index as low as 1.66 ± 0.32 during big flares. This behavior is not confirmed by the present analysis. The discrepancy is at the 2σ level (considering statistical errors only). The reason for this discrepancy remains unclear. The systematic uncertainty affecting the AGILE results may possibly be a factor. (The advertized uncertainty is 10% on the flux in Pittori et al. (2009), it may be fairly large in the photon index as well.)

The maximum photon energy found within the 95% containment radius from the location of 3C 454.3 during the period MJD 55,140–55,261 was a photon with $E = 20.7$ GeV at MJD 55,179.98, when $F_{E>100\,\rm MeV} = 6 \times 10^{-6}$ photon cm^{-2} s^{-1} and the variability time $t_{\rm var} \approx 1$ d. On MJD 55,167 (December 2), when the average of $F_{E>100\,\rm MeV}$ over this day exceeded $\approx 20 \times 10^{-6}$ photon cm^{-2} s^{-1}, the highest energy was 8.5 GeV. As already noted, the flux variations during this flare were on timescales as short as a few hours or less. The energy of the most energetic photon during periods of rapid flux changes provides the strongest constraint on the $\gamma\gamma$ opacity, as discussed below.

4. DISCUSSION

Thanks to this series of outbursts observed with the *Fermi*-LAT, a much more accurate picture of the behavior of 3C 454.3 in flaring states has been obtained. The unprecedented correlated spectral and flux variability studies in the γ-ray band enabled by the high observed flux have revealed interesting features (universality of the PSDs for time scales from a few hours to several months, mild spectral variability, weak change in the spectral break with flux), which can reasonably be assumed to apply to some extent for many flaring FSRQs. However,

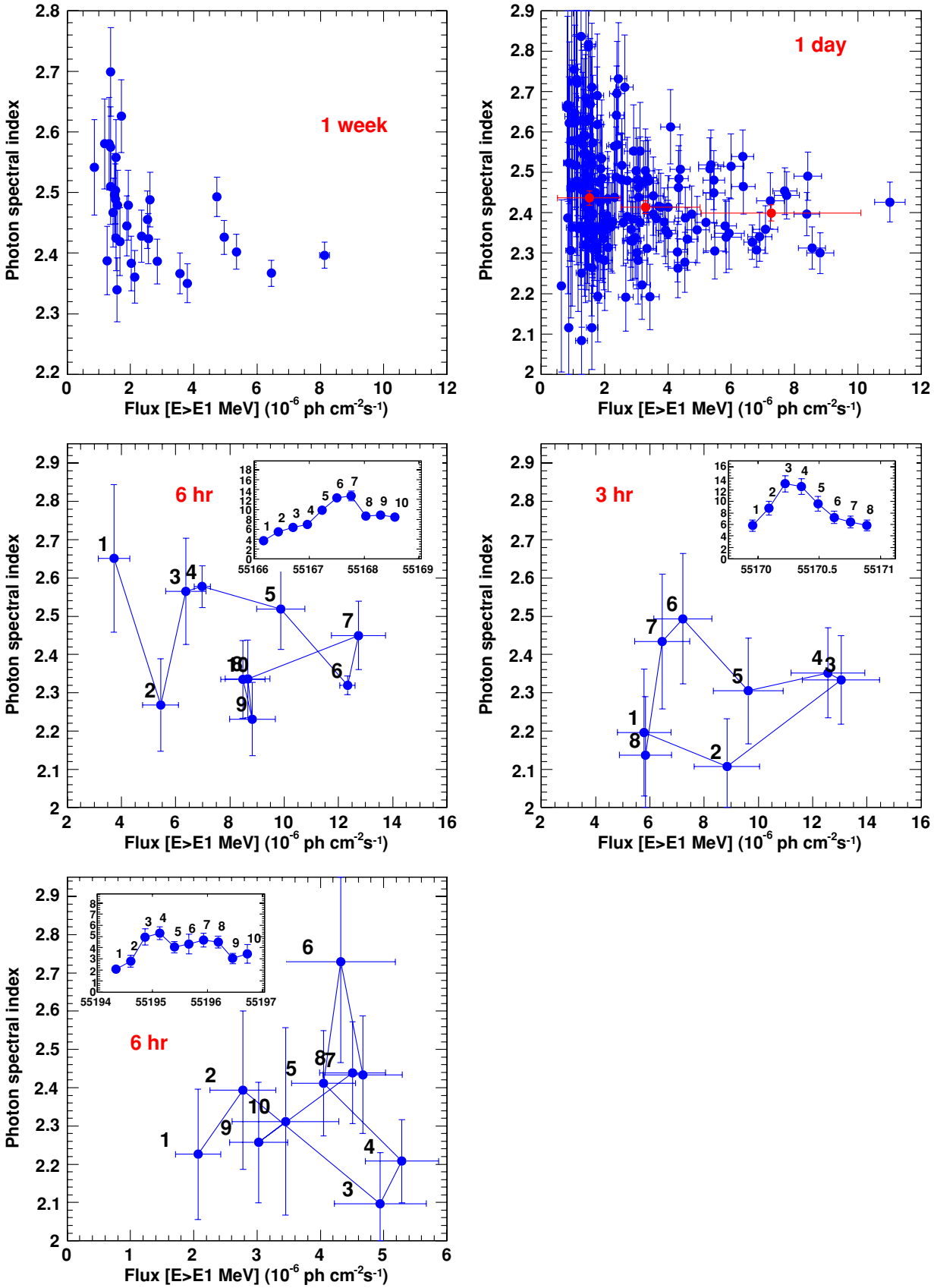

Figure 5. Photon spectral index vs. flux above E_1 (the photon energy where the correlation between integrated flux and index is minimal) measured on a weekly (upper left) and daily (upper right) basis are shown by blue points. The averages over periods with daily fluxes $F_{E_1} < 2.5$, $2.5 < F_{E_1} < 5$, $5 < F_{E_1} < 10$, where F_{E_1} is the photon flux above E_1 in units of 10^{-6} photon cm^{-2} s^{-1}, are shown by the red data points in the upper right panel. Middle left, middle right, and bottom panels show photon index vs. flux for the MJD 55,167, MJD 55,170 and MJD 55,195 flares, respectively. The labels refer to the different times of the light curve as shown in the insets.

(A color version of this figure is available in the online journal.)

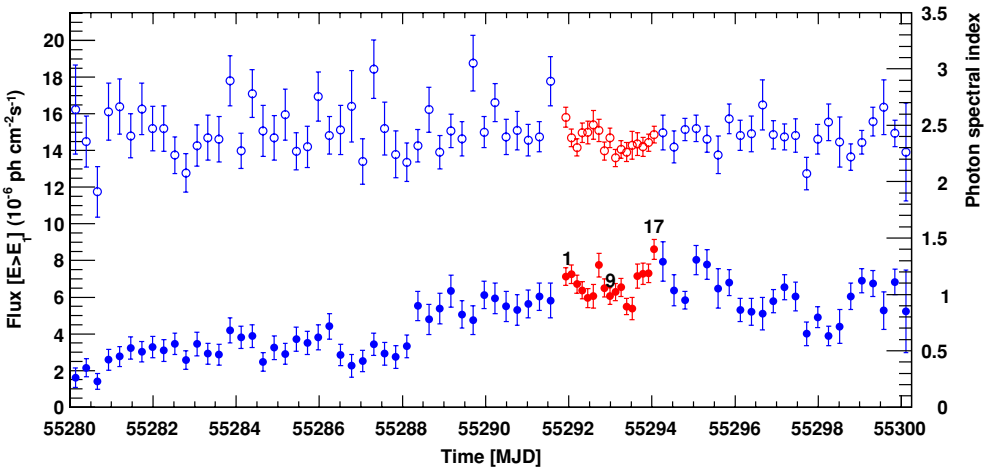

Figure 6. Flux (filled data points; left-hand axis) and photon index (open data points; right-hand axis) as a function of time in the period surrounding the ToO pointing. Data collected in the survey mode (6 hr binning) are in blue, those collected in pointed mode are in red (3 hr binning).
(A color version of this figure is available in the online journal.)

Table 1
Parameters of the Broken Power-law Functions, $N(E) \propto (E/E_{\rm break})^{-\Gamma_i}$, with $i = 1$ if $E < E_{\rm break}$ and $i = 2$ if $E > E_{\rm break}$, Fitted to the Spectra for the Different Periods Considered in Figure 8

Period	Flux [E>100 MeV] (10^{-6} photon cm^{-2}s^{-1})	Luminosity (10^{48} erg s^{-1})	Γ_1	Γ_2	$E_{\rm break}$ (MeV)	ΔL
1	3.45 ± 0.08	5.9	2.31 ± 0.02	3.19 ± 0.12	1810^{+250}_{-220}	−29.3
2	15.5 ± 0.5	27.2	2.33 ± 0.03	3.29 ± 0.21	2750^{+470}_{-360}	−15.5
3	4.40 ± 0.07	7.5	2.32 ± 0.02	3.12 ± 0.08	1600^{+150}_{-140}	−66.2
4	10.2 ± 0.2	17.1	2.38 ± 0.02	3.23 ± 0.14	2380^{+750}_{-280}	−50.7

Note. ΔL represents the difference of the logarithm of the likelihood with respect to a single PL fit.

Table 2
Parameters of the log Parabola Functions, $N(E) \propto E^{-\alpha-\beta\log(E/1GeV)}$, Fitted to the Spectra for the Different Periods Considered in Figure 8

Period	Flux [E>100 MeV] (10^{-6} photon cm^{-2}s^{-1})	Luminosity (10^{48} erg s^{-1})	α	β	ΔL
1	3.33 ± 0.08	5.9	2.52 ± 0.03	0.11 ± 0.02	−25.2
2	15.0 ± 0.5	27.1	2.48 ± 0.03	0.09 ± 0.02	−14.3
3	4.25 ± 0.07	7.4	2.54 ± 0.02	0.12 ± 0.01	−62.0
4	9.8 ± 0.2	16.8	2.55 ± 0.03	0.10 ± 0.02	−47.6

Note. ΔL represents the difference of the logarithm of the likelihood with respect to a single PL fit.

Table 3
Parameters of the Power-law +Exponential Cutoff Functions, $N(E) \propto E^{-\Gamma}\exp(-E/E_{\rm cutoff})$, Fitted to the Spectra for the Different Periods Considered in Figure 8

Period	Flux [E>100 MeV] (10^{-6} photon cm^{-2}s^{-1})	Luminosity (10^{48} erg s^{-1})	Γ	$E_{\rm cutoff}$ (MeV)	ΔL
1	3.42 ± 0.08	5.9	2.29 ± 0.03	5200 ± 900	−28.2
2	15.3 ± 0.5	26.8	2.25 ± 0.04	7000 ± 1700	−15.5
3	4.37 ± 0.07	7.4	2.24 ± 0.03	5200 ± 600	−63.9
4	10.1 ± 0.2	17.0	2.30 ± 0.03	7000 ± 1300	−51.4

Note. ΔL represents the difference of the logarithm of the likelihood with respect to a single PL fit.

the verification of this assertion might be difficult given the exceptional character of the fluxes considered here. Because of the *Fermi*-LAT characteristics, sources with a spectrum harder than that of 3C 454.3 can potentially be studied with a similar accuracy at a significantly lower flux, but only relatively few FSRQs have harder spectra than 3C 454.3 (Abdo et al. 2010b).

A photon flux of $F_{E>100\,\rm MeV} = 22 \pm 1 \times 10^{-6}$ photon cm^{-2} s^{-1} from 3C 454.3 at $z = 0.859$ implies an apparent isotropic γ-ray luminosity above 100 MeV of $L_\gamma \cong 3.8 \pm 0.2 \times 10^{49}$ erg s^{-1}. This is ∼3 times larger than the luminosity of the $z = 1.839$ blazar PKS 1502+106 during its 2008 August flare (Abdo et al. 2010c), but still lower than the luminosity of PKS 1622−297

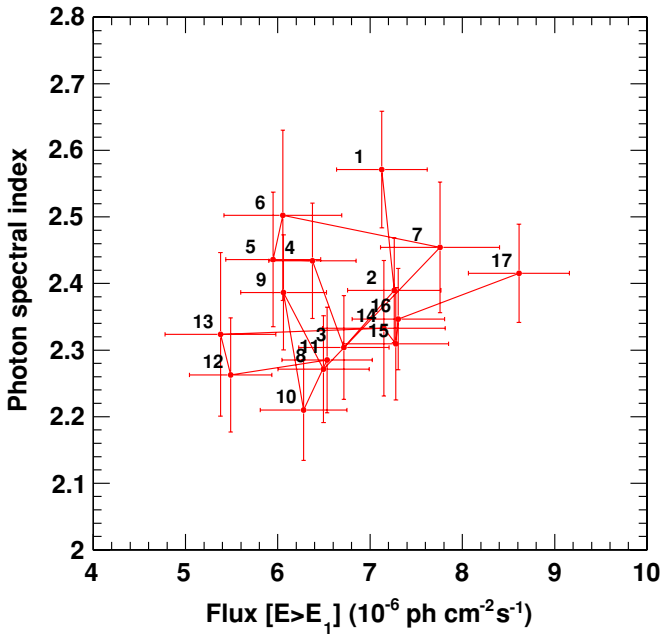

Figure 7. Photon spectral index vs. flux on 3 hr timescales during the time of the ToO pointing.

(A color version of this figure is available in the online journal.)

($\sim 5.1 \times 10^{49}$ erg s^{-1} with the current cosmological model) during the 1995 flare (Mattox et al. 1997). The time-averaged γ-ray luminosity (Tables) measured with the *Fermi*-LAT is $\approx 9 \times 10^{48}$ and $\approx 1.6 \times 10^{49}$ erg s^{-1} for periods 1 and 2, respectively. When written in units of $10^9 M_9$ Solar masses, estimates for the black-hole mass in 3C 454.3 range from $M_9 \approx 0.5$ (Bonnoli et al. 2010) to $M_9 \approx 4$ (Gu et al. 2001). To be radiating below the Eddington luminosity of $1.26 \times 10^{47} (M_9\, M_\odot)$ erg s^{-1} implies that the high-energy radiation is beamed into a jet with an opening angle $\theta_j \lesssim 0.1$.

The light curves from Figure 1 show evidence for a variability timescale of a few hours and the model fitted to a very brief subflare at MJD 55,170 implies a flux doubling timescale of $(\ln 4) \times T_r \sim 2.3$ hr. However, if the bulk of the flare were characterized with such a short timescale, we would expect a very erratic light curve calculated with daily binning. Because the overall shape of the 2009 November/December flare is smooth, the dominating variability timescale is rather close to $t_{\rm var} \sim 1$ d. The short subflares may reflect existence within or outside the main emitting zone of geometrical substructures with comoving emission-region sizes smaller than

$$R' \approx \frac{\delta c t_{\rm var}}{(1+z)} \approx 3.3 \times 10^{15} \left(\frac{\delta}{25}\right)\left(\frac{t_{\rm var}}{2.3\,{\rm hr}}\right) {\rm cm} \approx \frac{22}{M_9}\left(\frac{\delta}{25}\right)\left(\frac{t_{\rm var}}{2.3\,{\rm hr}}\right) R_{\rm g},$$

where $R_g = GM/c^2$ is the gravitational radius, $\delta \equiv [\Gamma_b(1 - \beta\cos\theta)]^{-1}$ is the Doppler factor, Γ_b is the bulk Lorentz factor and $\beta c = c\sqrt{1-(1/\Gamma_b^2)}$ is the speed of the jet plasma, and θ is the angle between the jet axis and observer's line of sight.

The minimum Doppler factor $\delta_{\rm min}$ is defined by the condition that the optical depth $\tau_{\gamma\gamma}(\epsilon_1)$ of a photon with energy $E_1 = \epsilon_1 m_e c^2$ to the $\gamma\gamma$ pair-production process is $\tau_{\gamma\gamma}(\epsilon_1) = 1$, and can be estimated to $\approx$10% accuracy for target photon number indices < -1 compared to results of more detailed numerical calculations through the expression

$$\delta_{\rm min} \cong \left[\frac{\sigma_T d_L^2 (1+z)^2 f_{\hat{\epsilon}} \epsilon_1}{4 t_{\rm var} m_e c^4}\right]^{1/6} \quad (2)$$

(Dondi & Ghisellini 1995; Ackermann et al. 2010). Here f_ϵ is the νF_ν spectrum of 3C 454.3 measured at frequency $\nu = m_e c^2 \epsilon / h$. To estimate $\delta_{\rm min}$, the photon with maximum energy E_1 is used during the period in which f_ϵ and variability time $t_{\rm var} = t_{\rm var,d}$ d are measured. The νF_ν flux f_ϵ in Equation (2) is evaluated at $\epsilon = \hat{\epsilon} = 2\delta^2/(1+z)^2\epsilon_1$ from the pair-production threshold condition $\epsilon\epsilon' \approx 2$, where primes on quantities refer to values measured in the comoving frame, so $\epsilon'_{(1)} = (1+z)\epsilon_{(1)}/\delta$. Writing $f_\epsilon = 10^{-10} f_{-10}$ erg cm^{-2} s^{-1} in Equation (2) gives $\delta_{\rm min} \approx 13[f_{-10}\, E_1({\rm 10GeV})/t_{\rm var,d}]^{1/6}$ and $\hat{E}({\rm keV}) \cong 9.5(\delta/25)^2/E_1({\rm 10\ GeV})$. *Swift*/XRT observations contemporaneous with the time that the 20 GeV photon was detected show a $\nu F_\nu \approx 3$ keV X-ray flux $\approx 5 \times 10^{-11}$ erg cm^{-2} s^{-1} (e.g., Bonnoli et al. 2010), so that $\delta_{\rm min} \approx 13$.

The value of the Doppler factor can also be constrained from the argument that the energy flux from the SSC component should be below that observed at soft X-rays, in terms of isotropic luminosities $L_{\rm SSC} \leqslant L_{\rm X}$. SSC luminosity is related to the synchrotron (SYN) luminosity via $L_{\rm SSC}/L_{\rm SYN} \sim u'_{\rm SYN}/u'_{\rm B}$ in the Thomson limit, where $u'_{\rm SYN} \sim L'_{\rm SYN}/(4\pi R'^2 c)$ is the energy density of synchrotron radiation and $u'_{\rm B} = B'^2/8\pi$ is the energy density of the magnetic field. Noting that Lorentz transformation of bolometric luminosity is $L_{\rm SYN} = \delta^4 L'_{\rm SYN}$, we obtain

$$\delta^6 \geqslant \frac{2(1+z)^2 L_{\rm SYN}^2}{L_{\rm X} c^3 t_{\rm var}^2 B'^2}. \quad (3)$$

This can be combined with a constraint from the EC and synchrotron luminosities ratio,

$$\frac{L_{\rm EC}}{L_{\rm SYN}} \sim \delta^2 \frac{u_{\rm EXT}}{u'_{\rm B}} \quad (4)$$

(Dermer 1995), where $u_{\rm EXT}$ is the energy density of external radiation. Eliminating from these equations the magnetic field value, we obtain

$$\delta \geqslant 17.6 \left(\frac{L_{\rm SYN}}{10^{48}\,{\rm erg\,s^{-1}}}\right)^{1/8} \left(\frac{L_{\rm EC}}{10^{49}\,{\rm erg\,s^{-1}}}\right)^{1/8} \times \left(\frac{L_{\rm X}}{10^{47}\,{\rm erg\,s^{-1}}}\right)^{-1/8} t_{\rm var,d}^{-1/4} \left(\frac{u_{\rm EXT}}{0.015\,{\rm erg\,cm^{-3}}}\right)^{-1/8}. \quad (5)$$

On the other hand, we can eliminate the Doppler factor and obtain a lower limit on the magnetic field

$$B'({\rm G}) \geqslant 3.4 \left(\frac{L_{\rm SYN}}{10^{48}\,{\rm erg\,s^{-1}}}\right)^{5/8} \left(\frac{L_{\rm EC}}{10^{49}\,{\rm erg\,s^{-1}}}\right)^{-3/8} \times \left(\frac{L_{\rm X}}{10^{47}\,{\rm erg\,s^{-1}}}\right)^{-1/8} t_{\rm var,d}^{-1/4} \left(\frac{u_{\rm EXT}}{0.015\,{\rm erg\,cm^{-3}}}\right)^{3/8}. \quad (6)$$

Order-of-magnitude reference values of isotropic luminosities $L_{\rm SYN}$, $L_{\rm X}$, and $L_{\rm EC}$ have been deduced from Figure 4 in Bonnoli et al. (2010). If the source region is located within the BLR, the energy density of external radiation is $u_{\rm EXT} \sim L_{\rm BLR}/(4\pi r_{\rm BLR}^2 c)$, where $L_{\rm BLR}$ is the luminosity of the broad

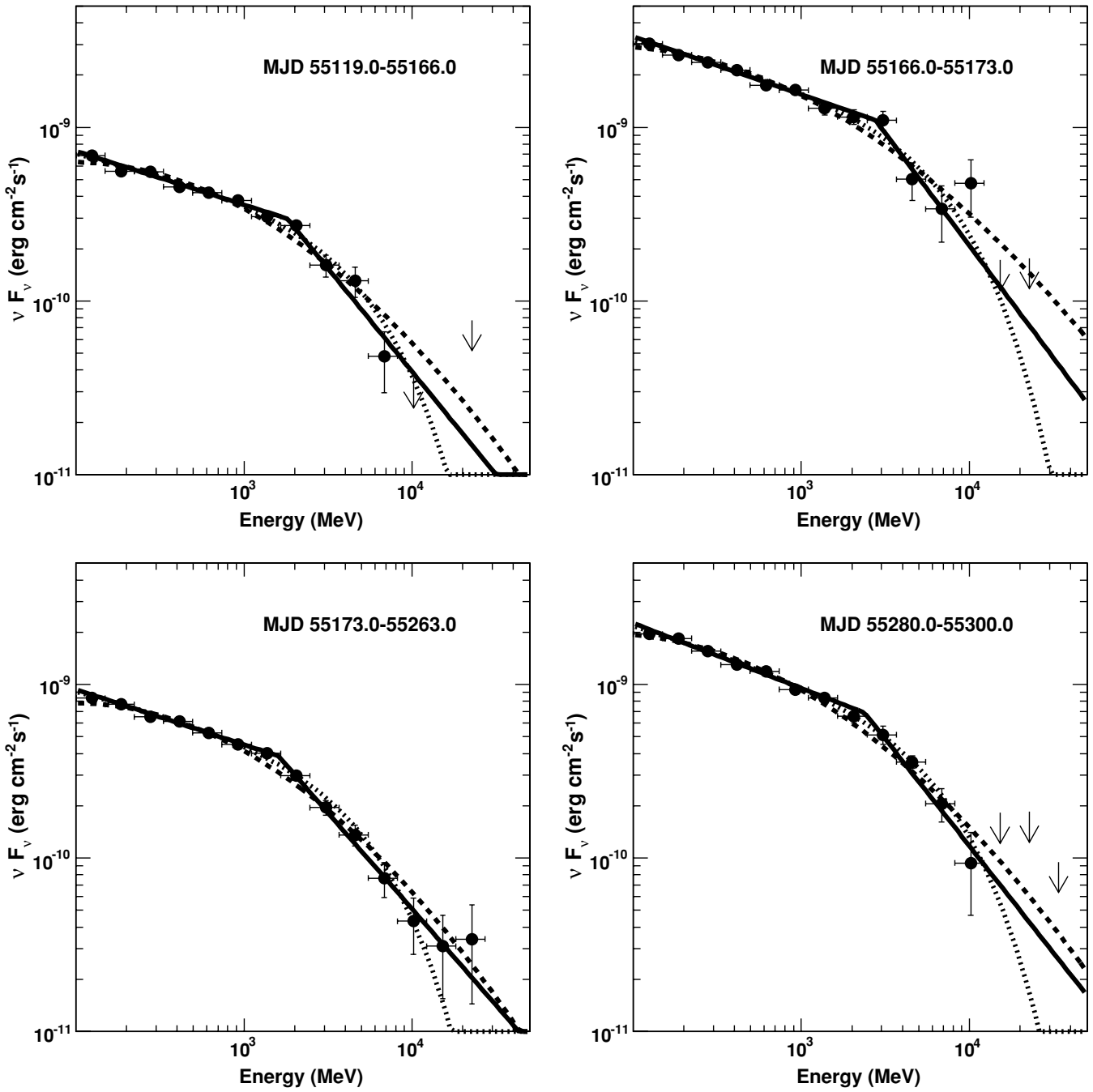

Figure 8. νF_ν distributions of the *Fermi*-LAT data for different time periods, along with the fitted BPL (solid), log parabola (dashed), and PL+exponential cutoff (dotted) functions.

emission lines and $r_{\rm BLR}$ is the characteristic radius of the BLR. We approximate $L_{\rm BLR}$ with *GALEX* measurement of Lyα line, $L_{{\rm Ly}\alpha} \approx (2\text{–}4) \times 10^{45}$ erg s^{-1} and adopt $r_{\rm BLR} \approx 6 \times 10^{17}$ cm based on reverberation scaling relations for C IV line (Bonnoli et al. 2010; Kaspi et al. 2007).

If the emission region is found deep within the broad-line region, the accretion-disk radiation can provide the dominant target photon source for γ-ray production. The target photon energy density is very sensitive to the BLR radius. Steady Lyα radiation as observed, e.g., in nearby radio-quiet AGN (Kaspi et al. 2007) could reflect a large radius for Lyα line photons, so other line radiations such as C IV λ1549 would instead dominate as the target photon source. In this case, $u_{\rm EXT}$ and the magnetic field given by Equation (6) would be smaller. Lower estimates of $u_{\rm EXT}$ imply smaller values of B'. Accretion-disk photons could make an important external radiation field, which would determine the magnetic field according to its contribution to $u_{\rm ext}$ and different estimates for the line fluorescence and scattered radiation fields. The Doppler factor is, however, still determined by the minimum value derived from gamma–gamma constraints, so it does not change much even if accretion disk photons make up the dominant target photon source, because internal SSC photons provide the dominant gamma–gamma opacity.

The analysis of radio observations made at a different epoch gives $\delta = 24.6 \pm 4.5$, bulk Lorentz factor $\Gamma_b = 15.6 \pm 2.2$, and observing angle $\theta = 1\overset{\circ}{.}3 \pm 1\overset{\circ}{.}2$ obtained from superluminal observations (Jorstad et al. 2005). Both our constraints on the Doppler factor are consistent with this result and would become

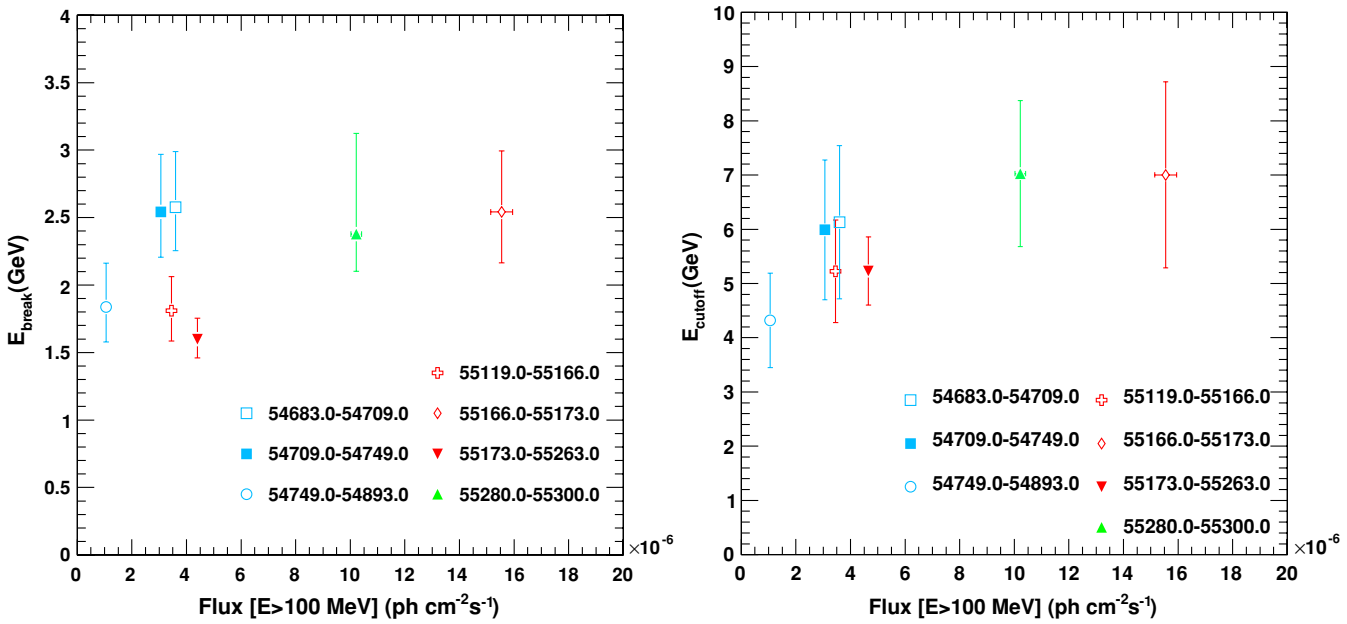

Figure 9. Left: $E_{\rm break}$ vs. flux for different time periods (given in MJD). Right: $E_{\rm Cutoff}$ vs. flux for the same time periods.
(A color version of this figure is available in the online journal.)

even tighter, if we adopt a shorter variability timescale. Hence, we take $\delta_{25} = \delta/25 \approx 1$ and $\Gamma_{15} = \Gamma_b/15 \approx 1$. The constraint on the value of the magnetic field B' is a few times the equipartition magnetic field $B'_{\rm eq}({\rm G}) \approx 2\,(f_{-10}\Lambda_2)^{2/7}\,/(\delta_{25}^{13/7}\nu_{13}^{1/7}t_{\rm var,d}^{6/7})$, where $f_{\rm SYN,peak} = 10^{-10} f_{-10}$ erg cm^{-2} s^{-1} is the observed synchrotron peak flux, $\nu_{\rm SYN,peak} = 10^{13}\nu_{13}$ Hz is the synchrotron peak frequency, and $100\Lambda_2 = (1+\zeta_{pe})\ln(\epsilon_2/\epsilon_1)$. Here ζ_{pe} is the ratio of proton to electron energy, and ϵ_1 and ϵ_2 bracket the $\nu F_\nu \propto \nu^{1/2}$ portion of the SED from electron synchrotron radiation (e.g., Finke et al. 2008). The equipartition magnetic field is ≈3.7× smaller in a pure lepton jet.

For a conical geometry of the opening angle $\theta_j \gtrsim R/r \sim 1/\Gamma_b$, the location of the emitting region for the December flare is constrained to be at a distance $r \lesssim 2c\Gamma_b^2 t_{\rm var}/(1+z) \approx 0.2\Gamma_{15}^2 t_{\rm var,d}$ pc; i.e., toward the outer parts of the BLR. A narrow jet with an opening angle $\lesssim 0.2/\Gamma_b$, places the emitting region further out, and could be consistent with a fragmentation of outflow (Marscher & Jorstad 2010). The most rapidly varying flaring episodes suggest locations at the sub-pc scale, contrary to conclusions from coherent optical polarization changes in 3C 279 (Abdo et al. 2010e) and PKS 1510-089 (Marscher et al. 2010) over timescales of tens of days, which suggest that the emitting regions are several pc from the black hole. Larger distances would be inferred if $\Gamma_b \gg 15$ or $\theta_j \ll 1/\Gamma_b$. Higher bulk Lorentz factors would conflict with the expected source density of the parent population of FSRQs, as we discuss later. Narrow jets are suggested by radio observations (Pushkarev et al. 2009; Jorstad et al. 2005) and could result from recollimation shocks at the pc scale (e.g., Nalewajko & Sikora 2009; Bromberg & Levinson 2009) that reduce the characteristic size of the emission region. A multiwavelength radio, mm, optical, and X-ray campaign covering observations of 3C 454.3 between 2005 and 2008 show coherent optical and mm flux and polarization episodes consistent with the brightest events taking place at the mm core located ∼ pc beyond the acceleration and collimation zone (Jorstad et al. 2010). Without strong collimation or recollimation, the short observed variability timescale implies a very small value $\theta_j \sim 2\times10^{-3} t_{\rm var,d}/r_{\rm pc}$ (Tavecchio et al. 2010) with an associated low radiative efficiency. Alternately, flaring episodes with short variability times might take place within the BLR, whereas the more slowly varying emissions could be radiated by jet plasma at larger distances. Spectral variations due to the different target photon sources might be concealed by mixing from components made at small and large radii. "Residual" collisions at large radii might also make a slowly varying underlying emission components, as similarly inferred for GRB observations (Li & Waxman 2008).

The large changes in flux exhibited by the γ-ray light curves in Figure 1 could be due to several different factors, including a changing mean magnetic field, electron number, Doppler factor, target photon density, and spectrum as the jet moves outward, or some combination of these factors. Any such explanation must also account for the moderate spectral changes, including the near constancy of $E_{\rm break}$ (Figure 9), while the flux changes by over an order of magnitude.

One possibility is related to scattering of a target photon field in the Klein–Nishina (KN) regime. Compton scattering takes place in the Thomson limit when the energy of the photon to be scattered is (in $m_e c^2$ units) $\epsilon'' \lesssim 1/4$ in the electron rest frame, denoted by the double primes on quantities. Since the radiation from ultrarelativistic electrons is seen only when they are moving very close to the line of sight, that energy for $\gamma \gg \Gamma_b$ is $\epsilon'' \simeq \gamma\delta\epsilon_\star$, where $\epsilon_\star$ is the average energy of the target photons in the lab frame. Hence, the scattering is in the Thomson regime provided the upscattered photon energies are $\epsilon_C \simeq (4/3)\delta^2\gamma^2\epsilon_\star/(1+z) \lesssim 1/[12\epsilon_\star(1+z)]$, i.e., for $E_C({\rm GeV}) \lesssim 12/E_\star({\rm eV})$, independent of the Doppler factor (compare Georganopoulos et al. 2001).

If the break energy observed in 3C 454.3 at ≈2 GeV is due to the transition to scattering in the KN regime, then the underlying target photon energy $E_\star \approx 6$ eV is close to the energy of the Lyα photon at 10.2 eV. We have tested this possibility by comparing the Compton-scattered spectrum from a PL electron distribution with a monochromatic Lyα photon source with the *Fermi*-LAT data. The spectrum is independent of δ, though it can depend on

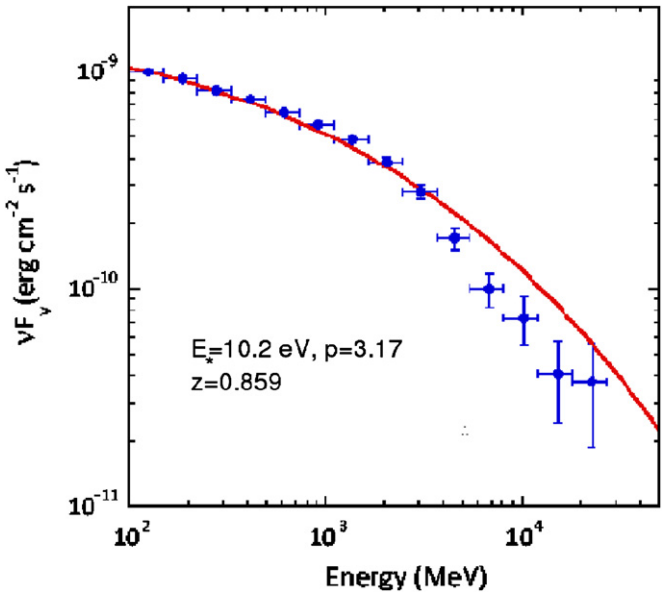

Figure 10. Model for the γ-ray spectrum of 3C 454.3 when a PL electron distribution Compton scatters Lyα photons. Best-fit electron number index $p = 3.17$. Model is insensitive to values of lower and upper comoving electron Lorentz factors $\gamma_{\rm min}$ and $\gamma_{\rm max}$ provided $\gamma_{\rm min} \lesssim 10^2$ and $\gamma_{\rm max} \gtrsim 10^4$. The KN softening from a PL electron distribution gives a poor fit to the data.

(A color version of this figure is available in the online journal.)

maximum and minimum electron Lorentz factors. As shown in Figure 10, the spectrum is too hard to fit the data and treatment of KN effects on cooling (Dermer & Atoyan 2002; Moderski et al. 2005; Sikora et al. 2009) or the addition of other soft photon sources will reduce the sharpness of the break. The difficulty of fitting the sharp spectral break with a single PL electron distribution is in accord with the conclusion of Abdo et al. (2009) that this break reflects a complex electron spectrum. To obtain a good spectral fit to the γ-ray spectrum of 3C 454.3, Finke & Dermer (2010) use a BPL electron distribution and a multi-component Compton-scattering model. The robustness of $E_{\rm break}$ in this model is due to similar, $\approx r^{-3}$ dependence of accretion disk and external radiation energy density within the BLR.

Although Abdo et al. (2009) excluded the possibility of explaining the spectral break with photon–photon pair absorption, Poutanen & Stern (2010) proposed that significant intrinsic absorption can be provided by He II Lyα line at 40.8 eV and continuum at 54.4 eV. However, their model implies that the location of the gamma-ray production is in the inner edge of the BLR and inefficient scattering in the KN regime is predicted to lead to significant hardening of synchrotron spectra in IR/optical bands. Further studies are required to verify whether such effect is in contradiction with multiwavelength spectra created within a one-zone model.

If $\Gamma_b \cong 15$ and the jet opening angle $\theta_j \approx 1/\Gamma_b$, then the beaming factor for a two-sided top-hat jet is $f_b \cong 1/2\Gamma_b^2 \cong 1/(450\Gamma_{15}^2)$. Within the framework of the unification hypothesis for radio galaxies (Urry & Padovani 1995), FRII radio galaxies are the parent population of FSRQs. The space density of FRII radio galaxies at $0.8 < z < 1.5$ is $\rho \cong 3 \times 10^{-7}$ Mpc^{-3} (Gendre et al. 2010). At redshift unity, the volume of the universe $\cong 4\pi/3R_H^3 \cong 3 \times 10^{11}$ Mpc^3. Therefore, if all FRII radio galaxies were misaligned FSRQs similar to 3C 454.3, then the implied number N of FSRQs is $N < f_b \times 3 \times 10^{-7}$ Mpc$^{-3} \times 3 \times 10^{11}$ Mpc$^3 \approx 200/\Gamma_{15}^2$. This number is similar to the number, $\approx$100, of γ-ray blazars at redshift unity (Abdo et al. 2010b), so it is in accord with the unification scenario. This simple argument suggests that unless $\theta_j \gg 1/\Gamma_b$, in which case the total jet energy of an individual FSRQ blazar would be correspondingly larger, the typical bulk Lorentz factor Γ_b for FSRQs would not be $\gg$15.

5. SUMMARY

The correlated spectral and temporal properties of 3C 454.3 during two very strong flaring episodes, during which the source was the brightest object in the γ-ray sky, have been studied. An important result of this work is that the significant spectral break between $\approx$2 and 3 GeV in the γ-ray spectrum of 3C 454.3 is very weakly dependent on the flux state, even when the flux changes by an order of magnitude. The light curves during periods of enhanced activity in 2008 July–August and 2010 December show strong resemblance, with a flux plateau of a few days preceding the major flare. The spectral index measured on a daily basis shows a very moderate "harder when brighter" effect for fluxes measured at $E > E_1$, where $E_1 = 163$ MeV is chosen to minimize spurious correlations resulting from the choice of the low-energy bound on the range. However, the weekly spectral index displays a more significant variation, but not exceeding $\Delta\Gamma = 0.35$ when the flux varies by more than a factor of 10. Indication for a gradual hardening preceding a major flare and extending for several weeks is found. No recurring pattern in the photon spectral index/flux plane measured at $E > E_1$ during the course of flaring episodes has been identified as would be expected in acceleration and cooling scenarios. Flux variations of a factor of 2 have been observed over time scales as short as 3 hr, though only weak variability was observed during the time of the ToO pointing of the *Fermi Telescope* toward 3C 454.3.

From $\gamma\gamma$ opacity constraints, we derive a minimum Doppler factor $\delta_{\rm min} \approx 13$ from the flux, variability time, and highest energy photon measurements. This value is in accord with independent measurements of δ from superluminal motion observations (Jorstad et al. 2005). The behavior of the break energy has also been investigated. Spectral softening due to the onset of KN effects in Compton scattering, which is independent of the Doppler factor for a PL electron distribution, was considered as the origin of the γ-ray spectrum. The magnitude of the softening for such a model was found to be inadequate to fit the spectrum without introducing intrinsic breaks in the underlying electron spectrum. An independent estimate of δ and the comoving magnetic field B' of the emission region also give values of $\delta \gtrsim 15$; also $B' \gtrsim$ several G. The short flaring times suggest an origin of the gamma-ray emission region within the BLR, but possible recollimation shocks, small-scale reconnection events, or more complicated jet geometries are compatible with the production of gamma-ray emission from 3C 454.3 on the pc scale.

The *Fermi*-LAT Collaboration acknowledges generous ongoing support from a number of agencies and institutes that have supported both the development and the operation of the LAT as well as scientific data analysis. These include the National Aeronautics and Space Administration and the Department of Energy in the United States, the Commissariat à l'Energie Atomique and the Centre National de la Recherche Scientifique/Institut National de Physique Nucléaire et de Physique des Particules in France, the Agenzia Spaziale Italiana and the Istituto

Nazionale di Fisica Nucleare in Italy, the Ministry of Education, Culture, Sports, Science and Technology (MEXT), High Energy Accelerator Research Organization (KEK) and Japan Aerospace Exploration Agency (JAXA) in Japan, and the K. A. Wallenberg Foundation, the Swedish Research Council, and the Swedish National Space Board in Sweden. Additional support for science analysis during the operations phase is gratefully acknowledged from the Istituto Nazionale di Astrofisica in Italy and the Centre National d'Études Spatiales in France.

REFERENCES

Abdo, A. A., et al. 2009, ApJ, 699, 817
Abdo, A. A., et al. 2010a, arXiv:1004.0348
Abdo, A. A., et al. 2010b, ApJ, 715, 429
Abdo, A. A., et al. 2010c, ApJ, 710, 810
Abdo, A. A., et al. 2010d, ApJ, 710, 1271
Abdo, A. A., et al. 2010e, Nature, 463, 919
Ackermann, M., et al. 2010, ApJ, 716, 1178
Atwood, W. B., et al. 2009, ApJ, 697, 1071
Bonning, E., et al. 2009a, ATel, 2332, 1
Bonning, E. W., et al. 2009b, ApJ, 697, L81
Bonnoli, G., Ghisellini, G., Foschini, L., Tavecchio, F., & Ghirlanda, G. 2010, arXiv:1003.3476
Bromberg, O., & Levinson, A. 2009, ApJ, 699, 1274
Dermer, C. D. 1995, ApJ, 446, L63
Dermer, C. D., & Atoyan, A. M. 2002, ApJ, 568, L81
Dondi, L., & Ghisellini, G. 1995, MNRAS, 273, 583
Edelson, R. A., & Krolik, J. H. 1988, ApJ, 333, 646
Escande, L., & Tanaka, Y. T. 2009, ATel, 2328, 1
Finke, J. D., & Dermer, C. D. 2010, ApJ, 714, L303
Finke, J. D., Dermer, C. D., & Böttcher, M. 2008, ApJ, 686, 181
Foschini, L., Tagliaferri, G., Ghisellini, G., Ghirlanda, G., Tavecchio, F., & Bonnoli, G. 2010, arXiv:1004.4518
Fuhrmann, L., et al. 2006, A&A, 445, L1
Gendre, M. A., Best, P. N., & Wall, J. V. 2010, MNRAS, 404, 1719
Georganopoulos, M., Kirk, J. G., & Mastichiadis, A. 2001, ApJ, 561, 111
Ghisellini, G., Foschini, L., Tavecchio, F., & Pian, E. 2007, MNRAS, 382, L82
Giommi, P., et al. 2006, A&A, 456, 911
Gu, M., Cao, X., & Jiang, D. R. 2001, MNRAS, 327, 1111
Hartman, R. C., et al. 1999, ApJS, 123, 79
Jorstad, S. G., et al. 2005, AJ, 130, 1418
Jorstad, S. G., et al. 2010, ApJ, 715, 362
Kaspi, S., Brandt, W. N., Maoz, D., Netzer, H., Schneider, D. P., & Shemmer, O. 2007, ApJ, 659, 997
Kirk, J. G., & Mastichiadis, A. 1999, Astropart. Phys., 11, 45
Krimm, H. A., et al. 2009, ATel, 2330, 1
Li, Z., & Waxman, E. 2008, ApJ, 674, L65
Marscher, A. P., & Jorstad, S. G. 2010, arXiv:1005.5551
Marscher, A. P., et al. 2010, arXiv:1002.0806
Mattox, J. R., Wagner, S. J., Malkan, M., McGlynn, T. A., Schachter, J. F., Grove, J. E., Johnson, W. N., & Kurfess, J. D. 1997, ApJ, 476, 692
Moderski, R., Sikora, M., Coppi, P. S., & Aharonian, F. 2005, MNRAS, 363, 954
Nalewajko, K., & Sikora, M. 2009, MNRAS, 392, 1205
Pacciani, L., et al. 2010, ApJ, 716, L170
Peterson, B. M., Wanders, I., Horne, K., Collier, S., Alexander, T., Kaspi, S., & Maoz, D. 1998, PASP, 110, 660
Pittori, C., et al. 2009, A&A, 506, 1563
Poutanen, J., & Stern, B. 2010, ApJ, 717, L118
Pushkarev, A. B., Kovalev, Y. Y., Lister, M. L., & Savolainen, T. 2009, A&A, 507, L33
Sakamoto, T., D'Ammando, F., Gehrels, N., Kovalev, Y. Y., & Sokolovsky, K. 2009, ATel, 2329, 1
Sasada, M., et al. 2009, ATel, 2333, 1
Sikora, M., Stawarz, Ł., Moderski, R., Nalewajko, K., & Madejski, G. M. 2009, ApJ, 704, 38
Striani, E., et al. 2009a, ATel, 2322, 1
Striani, E., et al. 2009b, ATel, 2326, 1
Striani, E., et al. 2010, ApJ, 718, 455
Tavecchio, F., Ghisellini, G., Bonnoli, G., & Ghirlanda, G. 2010, MNRAS, 405, L94
Urry, C. M., & Padovani, P. 1995, PASP, 107, 803
Vercellone, S., et al. 2009a, ApJ, 690, 1018
Vercellone, S., et al. 2009b, ATel, 2344, 1
Vercellone, S., et al. 2010, ApJ, 712, 405
Villata, M., et al. 2006, A&A, 453, 817
Villata, M., Raiteri, C. M., Larionov, V. M., Konstantinova, T. S., Nilsson, K., Pasanen, M., & Carosati, D. 2009, ATel, 2325, 1